

Anodic Photocurrents and Corrosion Currents on Passive and Active-Passive Metals [☆]

T.D. Burleigh*

ABSTRACT

A photoelectrochemical study was made to compare Zr, Ti, Zn, Sn, Fe, and Cu in 1 N sulfuric acid and/or 1 N KOH. This group includes spontaneously passive, active-passive, and nonpassive metals. The apparent direct and indirect bandgaps and the flat-band potentials were measured for the anodic oxides of each metal. (The bandgaps and flat-band potentials can be used to identify the anodic oxide.) The corrosion currents and the photocurrents were compared. The photocurrent was generated by pulses of monochromatic light. Relationships are observed between the corrosion current and the photocurrent, notably for the formation of new oxides and the active-passive transition.

INTRODUCTION

Many researchers have reported that the passive oxide films on metals behave like semiconductors. Oshe and Rosenfel'd¹ used their photoelectric polarization method to measure whether the oxides on several metals were p-type or n-type. Delnick and Hackerman² used redox couples to develop a semiconductor model of the passive oxide on iron. A review by Stimming³ covers many papers that describe the use of photoelectrochemistry to study the passive oxides on metals. Peter⁴ has shown photoelectrochemical results for Pb, Cu, Fe, Ti, and Bi. However, a few researchers have also suggested that the semiconductor properties of the anodic oxide might control the corrosion resistance of the base metal. Vijn⁵ suggested this and showed a relation between the open-circuit corrosion potential in chloride solutions and the bandgap energy of the oxides of several metals. Sato⁶ compared nickel and iron in sulfuric acid and concluded that the n-type oxide was more stable against anodic breakdown than the p-type oxide. Burleigh and Latanision⁷ showed a relation between the corrosion resistance of glassy Cu-Zr and Cu-Zr-P alloys and polycrystalline Zr and their respective anodic oxide's flat-band potentials. This present paper compares several metal/electrolyte systems and suggests a connection between the photocurrent (or lack thereof) and passive or active dissolution.

The dominant mechanism of photocurrent for an n-type oxide on a metal is shown in Figure 1. (Most of the passivating oxides are n-type.)¹ Since these oxide films can be disordered and of

variable composition, they do not have a distinct bandgap energy (E_g) as would a single-crystal, bulk semiconductor. Thus additional energy levels are shown within the oxide's bandgap in Figure 1 to represent the imperfect nature of these thin oxide films.^{3,8} Illumination can create holes and electrons in the oxide if the incident photon's energy is large enough. Figure 1 illustrates sub-bandgap excitation between impurity levels, and also bandgap excitation between the lower valence band and the upper conduction band. The created holes and electrons flow in opposite directions because of the electric field in the oxide. This mechanism is generally used to explain the photocurrents generated from semiconductors immersed in electrolytes (Gerischer)⁹ and also for anodic photocurrents on metals.^{3,4} The contact between the metal and its oxide is assumed in this paper to be ohmic, and therefore is ignored. Figure 1 is a simplified picture since the actual situation could be more complex (e.g., see Gerischer).¹⁰

The quantum yield (Φ) is the number of electrons measured per incident photon. The square or the square root of the quantum yield may be plotted vs photon energy to obtain the apparent direct bandgap or indirect bandgap respectively. The x-axis intercept of the linear portion of the curve is defined as the direct bandgap for $h\nu$ vs Φ^2 , or the indirect bandgap for $h\nu$ vs $\Phi^{1/2}$. (The details for this calculation have been previously shown by Stimming³ and Peter.⁴ The bandgap energy can often be used to identify the surface oxide. Strehlow and Cook¹¹ have compiled the bandgap energies of many elemental and binary semiconductors and insulators. However, it is necessary to know whether the bandgap of the material is a direct or indirect transition.

Since the generation of a photocurrent depend on the presence of an electric field in the oxide, there will usually be a potential where the electric field goes to zero and the photocurrent disappears. In a crystalline semiconductor, this zero photocurrent potential is the so-named "flat-band potential" (V_{fb}). In a disordered anodic oxide the situation is more complex,¹⁰ but in this present paper the flat-band potential (V_{fb}) for the anodic oxides is defined as the potential where the onset of the photocurrent occurs.

In this paper, the corrosion current and the photocurrent for several metals are compared, and similarities are shown between the different metals. Results are shown for Zr in 1 N KOH and 1 N H₂SO₄, Ti in 1 N KOH and 1 N H₂SO₄, Zn in 1 N KOH, Sn in 1 N KOH, Fe in 1 N KOH and 1 N H₂SO₄, and Cu in 1 N KOH. The two test solutions, 1 N KOH and 1 N H₂SO₄, were chosen because they represent two extremes, an acid and a base, but in which the above metals can form stable anodic oxides.

* Submitted for publication July 1988; revised September 1988.

* Alloy Technology Division, Alcoa Laboratories, Alcoa Center, PA 15069.

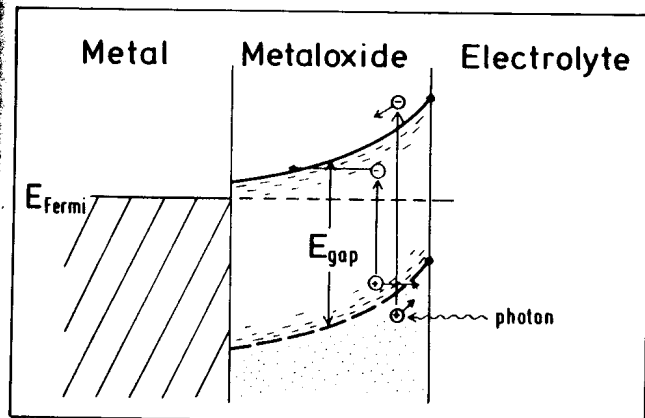


FIGURE 1. The photocurrent is caused by photons creating hole-electron pairs within the oxide layer. Because of the band-bending, the holes and electrons flow in opposite directions.

EXPERIMENTAL

The metals used in this research were high purity and polycrystalline in the form of rod or foil. The zirconium was 99.9% Zr foil. The titanium was 99.7% Ti foil. The zinc was 99.9985% Zn rod (7-mm diameter). The tin was 99.9985% Sn rod (6-mm diameter). The iron was 99.99% Fe foil. The copper was 99.999% Cu foil. The Cu, Ti, Zr, Sn, and Zn were obtained from Alfa Products.⁽¹⁾

Samples were prepared in the following manner: The metal sample was first mounted to a brass holder with conducting epoxy. The metal was then dry-polished to 400 grit Al_2O_3 , cleaned with methanol, and allowed to dry. The 400 grit polish was used as a simple and reproducible surface preparation for the different metals. The dried sample was masked with UHU⁽²⁾ Plus 300[†] epoxy to expose only a few square millimeters of surface area (the small surface area improved the signal-to-noise ratio). The epoxy was allowed to cure overnight or longer before immersion. The test solutions were either 1 N KOH or 1 N H_2SO_4 . Approximately 100 mL of solution were used per test. These solutions were made from triply distilled water and analytical grade KOH, or concentrated H_2SO_4 . The test solutions were deaerated before and during the test by nitrogen gas bubbling. All tests were made at room temperature. The photoelectrochemical apparatus is shown in Figure 2. The light shines from the xenon arc lamp (Osram⁽³⁾ XBO 150 w/1)[†] and through the Bausch & Lomb⁽⁴⁾ High Intensity[†] monochromator. The chopper chops the monochromatic light into pulses at 10 Hz. The chopped light shines through the quartz window and strikes the sample. The periodic photocurrent is separated from the dark corrosion current by the PAR⁽⁵⁾ Model HR-8 Lock-in Amplifier[†] and the photocurrent is recorded. The potentiostat was built at the Fritz-Haber-Institut in West Berlin.

The reference electrode was $Hg/Hg_2SO_4/0.5 M K_2SO_4$, and all voltages are reported relative to this. This Hg_2SO_4 reference electrode is 1420 mV positive to the reversible hydrogen electrode (RHE) in 1 N KOH and 690 mV positive to the RHE in 1 N H_2SO_4 . The Hg_2SO_4 reference electrode was used in preference to the standard calomel electrode (SCE) in order to avoid chloride contamination.

The voltammograms were cycled at 10 mV/s (20 mV/s for Cu) until the voltammograms were reproducible. In the voltammo-

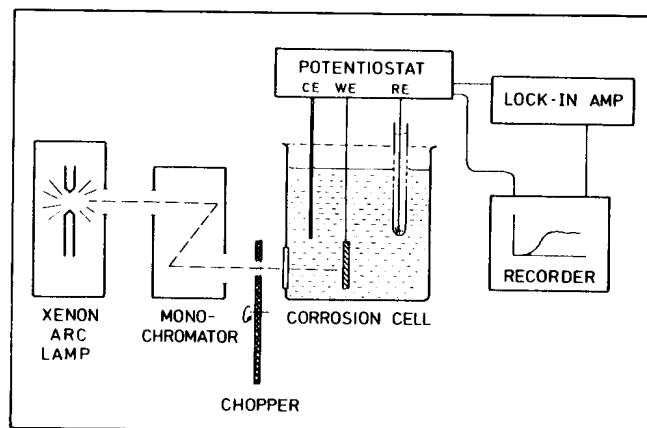


FIGURE 2. The photoelectrochemical experimental apparatus. The light shines from the xenon arc lamp, through the monochromator, chopper and quartz window, and strikes the immersed sample. The cyclic photocurrent is separated from the corrosion current by the lock-in amplifier.

gram, the corrosion current in the dark is the solid curve and its scale is labeled "Dark Current Density" on the left vertical axis. The "Photocurrent Density" is the dashed curve and its scale is on the right vertical axis.

The photocurrent spectra were measured after the metal had remained at the set potential for a period of time and the photocurrent spectrum was reproducible. This ensured that the oxide film was near steady state. It was only possible to measure the spectra near the steady state since it generally took fifteen minutes to sweep the monochromator through the wavelengths (at 20 nm/min) for a single spectrum. The spectrum for the metals might change for several hours or even a day after immersion. The quantum yield (Φ) is shown in the figures and was measured under parallel light. The quantum yield was obtained by dividing the photocurrent density by the power density of the xenon lamp and converting to electrons per incident photon. The power density of the xenon lamp was measured with parallel light passing through the same optical path (lenses, quartz windows, and 3 cm of solution). The illumination was measured with a Pyroelectric Radiometer Rk-5100[†] using the RkP 545[†] detector.⁽⁶⁾ Due to aberrations, it was found that the photospectra would shift slightly if a focused point of light was used rather than parallel light. Therefore, most of the photospectra were measured under parallel light, but the photocurrent voltammograms were measured under focused light for their increased magnitude. The intensity of the focused light was about 3 mW/cm² (at $\lambda = 400$ nm). The intensity of the parallel light was 0.1 mW/cm² (at $\lambda = 400$ nm).

EXPERIMENTAL RESULTS

Zirconium is spontaneously passive in the two test solutions. It has no anodic active dissolution region where its oxide film is unstable. The cyclic voltammogram for Zr in 1 N H_2SO_4 is shown in Figure 3. (This is also typical for Zr in 1 N KOH.) It can be seen that the photocurrent ($\lambda = 240$ nm) is almost linear vs the potential. The photocurrent reverses sign near -1.0 V, which is where the dark current is already negative (cathodic). The photospectra are shown in Figure 4. Previous photoelectrochemical work by the author¹² showed similar, though less accurate, results. In Figure 4(a), the quantum yield for Zr in 1 N KOH is 0.5%, while for Zr in 1 N H_2SO_4 it is 5%, ten times higher. (However, the corrosion currents are also ten times larger in the sulfuric acid.) In Figure 4(b), the plot of the direct E_g ($h\nu$ vs Φ^2) extrapolates to the same direct

⁽¹⁾ Alfa Products Division of Thiokol/Ventron, Danvers, MA.

⁽²⁾ UHU Vertrieb GmbH.

[†] Trade name.

⁽³⁾ Osram Corp., Newburgh, NY.

⁽⁴⁾ Bausch & Lomb Scientific Optical Products Division, Rochester, NY.

⁽⁵⁾ EG&G Princeton Applied Research (PAR) Corp., Princeton, NJ.

⁽⁶⁾ Laser Precision Corp., Utica, NY.

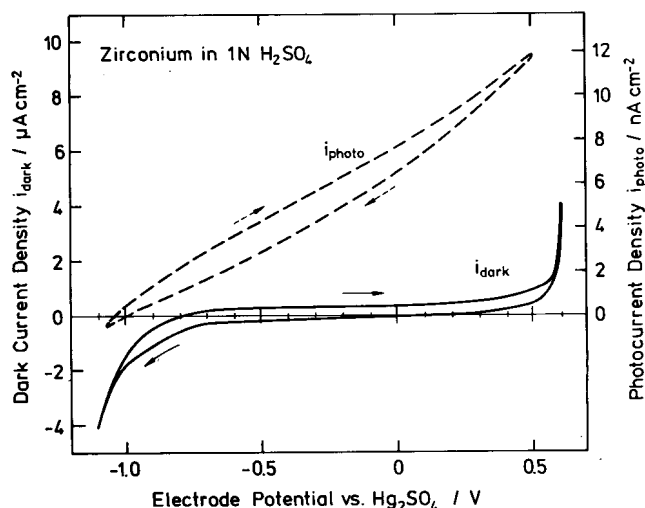
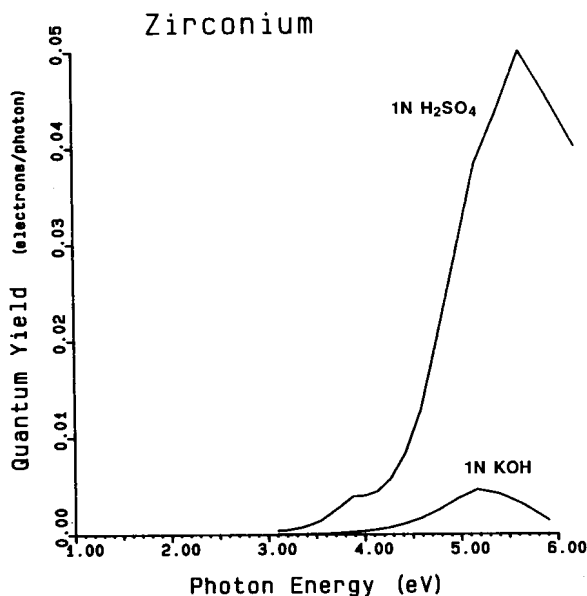


FIGURE 3. The cyclic voltammogram for zirconium in 1 N sulfuric acid (10 mV/s, $\lambda = 240$ nm). The photocurrent (right axis) is the dashed curve, and the dark corrosion current (left axis) is the solid curve.

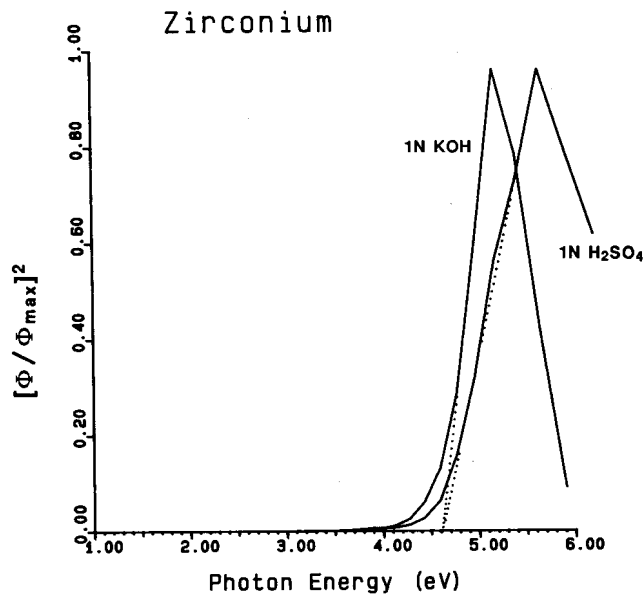
bandgap value (4.6 eV). This demonstrates that the anodic oxides for zirconium are the same in the acid or the base solutions. The apparent direct E_g and indirect E_g are tabulated in Table 1. The results for zirconium anodic oxide fit best assuming a direct bandgap. The bandgap of ZrO_2 (unspecified transition) has been reported as 4.99 eV.¹¹

These photospectra, and most of the photospectra shown here, exhibit tails extending into the lower energy region. These tails, also called Urbach tails,³ result from excitation of the impurity levels within the bandgap (shown in Figure 1) or perhaps electron injection from the surface. The decrease in the quantum yield at higher photon energies in Figure 4 is a real effect (see the results in the next section for titanium).

Titanium is also spontaneously passive in the two test solutions. The cyclic voltammogram for Ti in 1 N H_2SO_4 is shown in Figure 5(a), and for Ti in 1 N KOH is shown in Figure 5(b). The photocurrent ($\lambda = 300$ nm) goes to zero near the corrosion potential. The dark current in Figure 5(a) shows a peak near -0.7 V during the forward (positive) sweep, but this peak disappears in the potentiostatic test (data not shown here). Therefore, this current rise is not active dissolution but probably a hydrogen desorption current. Above $+0.5$ V the dark current increases. However, this is also not present in the potentiostatic polarization because the oxide film grows thicker to compensate for the increased voltage. Figure 6(a) shows the quantum yield for the anodic oxide on titanium and also for single-crystal TiO_2 rutile. Assuming the anodic oxide is indirect gap gives the most consistent fit to the data. The apparent indirect bandgap (Figure 6[b]) for the anodic oxide on titanium is $E_g(\text{ind}) = 3.2$ eV. This is similar to the value found by Schultze et al.¹³ and Leitner et al.¹⁴ However, the single-crystal rutile has an extrapolated $E_g = 2.9$ eV indirect gap (or 3.0 eV direct gap). This is in agreement with Cronemeyer's¹⁵ value of 3.05 eV for single-crystal rutile (Cronemeyer measured at the maximum photocurrent, and not the extrapolated value). Schultze et al.¹³ and Leitner et al.¹⁴ have noted this discrepancy in E_g and concluded that the anodic oxide's larger bandgap was a result of the anodic film being highly disordered and amorphous. However, a more likely explanation is that the anodic oxide on titanium is the anatase structure rather than the rutile structure. Work by Gusev et al.¹⁶ found the bandgap of rutile to be 3.02 eV, but anatase to be 3.23 eV. Clark¹⁷ similarly reports that rutile is transparent to $24,500\text{ cm}^{-1}$ (3.04 eV) but anatase is transparent to $\sim 26,000\text{ cm}^{-1}$ (3.22 eV). Blondeau et al.¹⁸ compared electron diffraction patterns of the TiO_2 anodic film with computed intensity distributions and they concluded that the anodic oxide consisted of plate-



a



b

FIGURE 4. The photospectra for zirconium in 1 N sulfuric acid (2.5 h at $+0.50$ V and $i_d = 5.1\ \mu\text{A}/\text{cm}^2$) and in 1 N KOH (4 h at $+0.00$ V and $i_d = 0.26\ \mu\text{A}/\text{cm}^2$). (a) In sulfuric acid the photocurrent is ten times larger, but then so is the dark corrosion current, i_d . (b) The oxide has the same direct bandgap ($h\nu$ vs Φ^2) in both solutions ($E_g = 4.6$ eV).

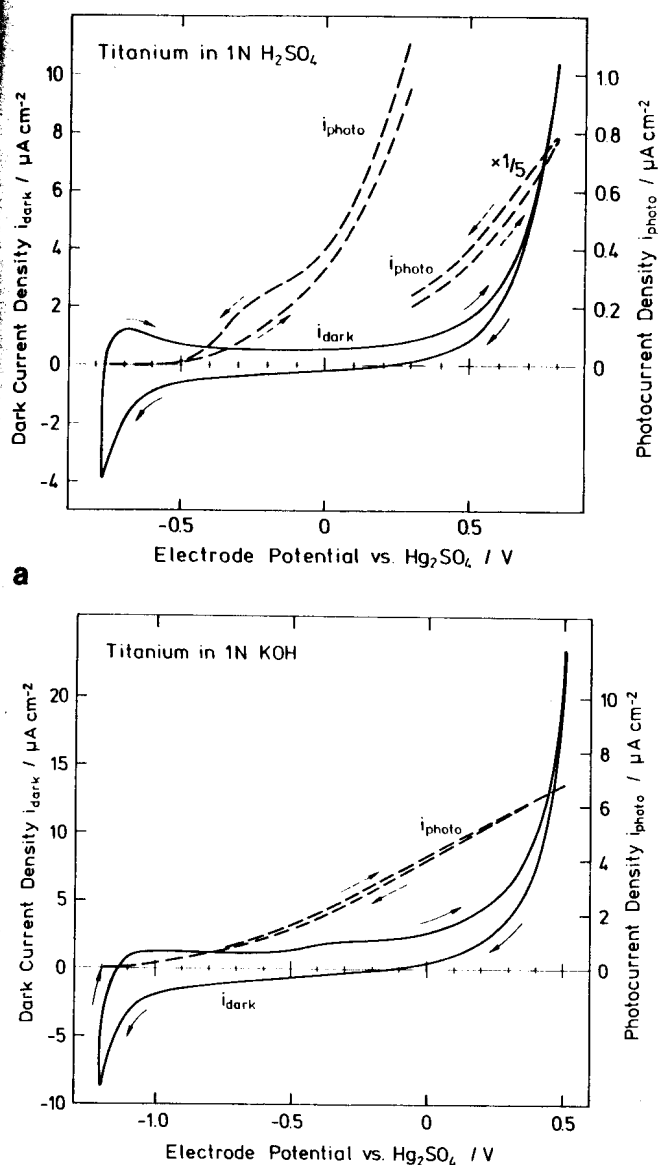
lets of 24 atoms built on the (112) plane of anatase. Yalalom and Zahavi¹⁹ have shown with electron diffraction that the titanium anodic film formed at 85 V had the anatase structure. Recent work by Kozlowski et al.²⁰ used reflection electron diffraction to determine the structure of low-voltage anodic oxides on titanium. The only identifiable phase Kozlowski et al.²⁰ found was rutile. After comparing the *in situ* bandgap measurements and the *ex situ* electron diffraction results, I hypothesize that the initial anodic oxide on titanium is most likely TiO_2 anatase, and not amorphous nor rutile. Anatase is less dense than rutile, but transforms to rutile upon heating.¹⁷ The thin anatase film could convert from anatase to rutile while in the vacuum and heated by the electron beam during electron microscopy.

TABLE 1
Semiconductor Properties of Anodic Oxides of Zr, Ti, Zn, Fe, and Cu in 1 N H₂SO₄ and/or 1 N KOH

Base Material	Electrolyte	Anodic Oxide	V _{fb} ^(A) (V)	E _g (Indirect) ^(B) (eV)	E _g (direct) ^(B) (eV)	Quantum Yield ^(B) (max %)	Transition
zirconium	1 N KOH	ZrO ₂	-1.5	3.8 to 3.9	4.6	0.5	direct
zirconium	1 N sulfuric	ZrO ₂	-1.2	3.8	4.6	5.0	direct
titanium	1 N KOH	TiO ₂ (anatase)	-1.2	3.2	3.6	4.0	indirect
titanium	1 N sulfuric	TiO ₂ (anatase)	-0.8	3.2	3.6 to 3.9	2.0	indirect
TiO ₂ rutile	1 N sulfuric	TiO ₂ rutile	-0.6	2.9	3.0	63.0	indirect
zinc	1 N KOH	Zn(OH) ₂ ?	-1.5	1.4	—	0.1	
zinc	1 N KOH	ZnO	-1.3	3.1	3.3	0.3	
ZnO polycryst.	1 N KOH	ZnO	-1.3	3.05	3.15	40.0	
iron	1 N KOH	(1) Fe(OH) ₃ ?	-1.0	(2.2 to 2.5)	(2.9 to 3.2)	(<0.02)	
iron	1 N KOH	(2) Fe ₂ O ₃ ?	?	2.0 to 2.2	2.7	0.1	
iron	1 N sulfuric	Fe ₃ O ₄ ?	0.4	(1.9 to 2.0)	(2.6 to 2.8)	—	
iron	1 N sulfuric	Fe ₂ O ₃ ?	?	(2.0 to 2.1)	(2.7 to 2.8)	—	
copper	1 N KOH	(1) p-Cu ₂ O	-0.7	2.4	—	(<0.1)	indirect
copper	1 N KOH	(2) p-CuO	-0.4	(1.1 to 1.7)	—	(<0.1)	indirect

^(A) The flat-band potential, V_{fb}, is measured vs Hg/Hg₂SO₄/0.5 M Na₂SO₄ reference electrode.

^(B) Numbers in parentheses are approximations.



In these and other photospectra, the quantum yield reaches a maximum and then decreases at higher photon energies. This is a real effect and it has been documented by others and is a cause of controversy,²¹ but it is beyond the scope of this paper.

Zinc is an active-passive metal. The cyclic voltammogram for Zn in 1 N KOH is shown in Figure 7. The active region for zinc is from -1.86 to -1.6 V, and here there is no photocurrent. The photocurrent ($\lambda = 350$ nm) begins in the passive region near -1.4 V (V_{fb}), and increases, with a crossover near -0.9 V. The photospectra are shown in Figure 8 with the photospectrum for polycrystalline ZnO included for comparison. The band-edge of the passive oxide on the surface of zinc at higher potentials closely corresponds to polycrystalline ZnO. Previous photocurrent vs potential work on zinc by Fruhwirth et al.²² also showed a similarity between the oxide on Zn metal and single-crystal ZnO in 0.1 M borax solution. Interestingly, in Figure 8, the quantum yield (Φ) for polycrystalline ZnO reaches a plateau for higher energy photons, but for the anodic oxide film, Φ peaks and then decreases rapidly, similar to the effect seen above for the anodic film on titanium. At -1.0 V, where there was the crossover in the photocurrent, the photospectrum is different. Perhaps a zinc hydroxide, with a smaller E_g and lower quantum efficiency, exists on the surface at -1.0 V. However, the stable anodic oxide at more positive potentials is ZnO since the two band-edges are identical.

Tin is also an active-passive metal. The cyclic voltammogram for Sn in 1 N KOH is shown in Figure 9. In 1 N KOH, there is a complicated oxide on the surface that can be photosensitive. Detailed results for tin are complex and are explained in a separate paper.⁸ The corrosion current (solid curve) and the photocurrent (dashed curve) in Figure 9 were measured simultaneously under intense illumination ($\lambda = 350$ nm, 2 mW/cm²). The tin sample had previously been held at -0.40 V for 20 hours under the intense illumination. This illumination was used to remove a photosensitive, nonprotective surface film, which confused the picture.⁸ The potentiostatic polarization curve (dotted curve) was a separate experiment in the dark. It was started at -1.60 V and increased in +100 mV steps and held at each step for several minutes until the corrosion current was constant and recorded. Noteworthy, the active dissolution region occurs at potentials more negative than the photocurrent onset potential (V_{fb}). Previous photoelectrochemical work on tin was reported by Kapusta and Hackerman.²³ They reported that at pH = 8.5, the anodic oxide on tin was a nonstoichiometric SnO₂ with a E_g (indirect) = 2.55 eV.

Iron is spontaneously passive in 1 N KOH, but active-passive in 1 N H₂SO₄. The cyclic voltammogram for Fe in 1 N KOH is shown in Figure 10. The corrosion current (dark) shows no active dissolution region. The photocurrent ($\lambda = 400$ nm) in Figure 10(a) shows a secondary maximum near -0.6 V. If after cycling the iron

FIGURE 5. The cyclic voltammograms for titanium in 1 N KOH and 1 N sulfuric acid (10 mV/s, $\lambda = 300$ nm).

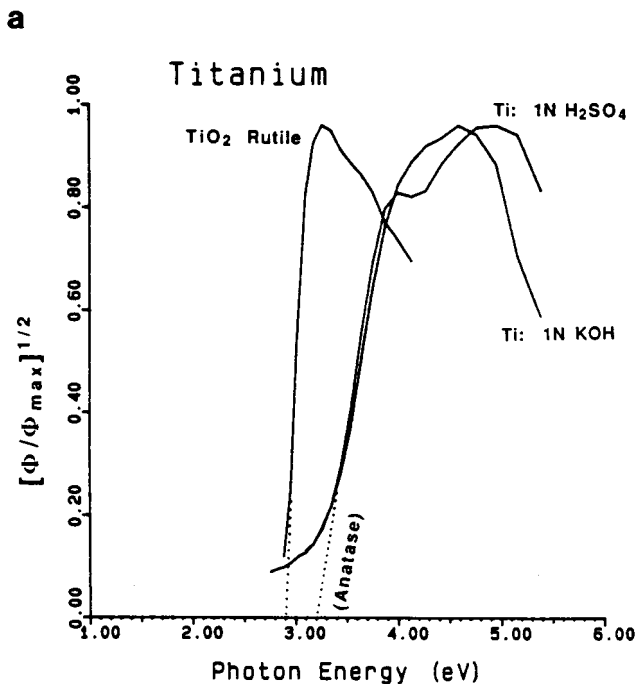
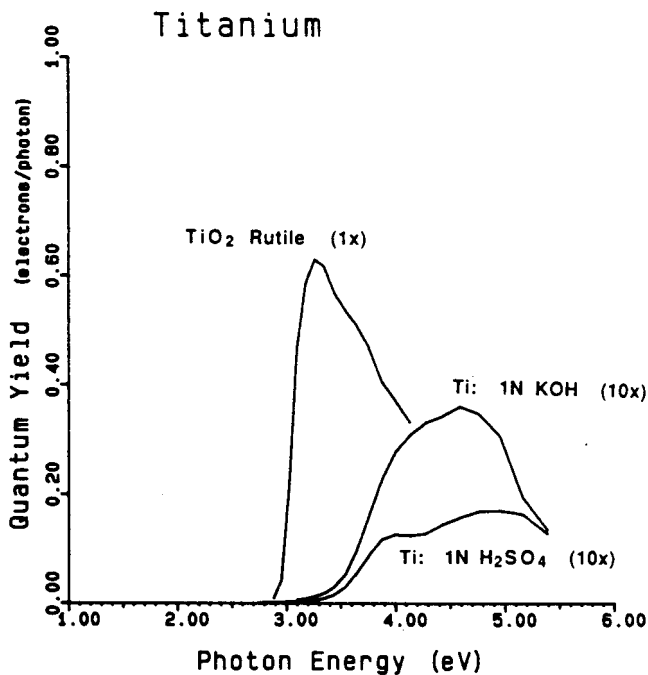


FIGURE 6. The photospectra for the anodic oxide on titanium in 1 N sulfuric acid (12 h at +0.50 V and $i_d = 0.75 \mu A/cm^2$) and 1 N KOH (24 h at +0.00 V and $i_d = 5.6 \mu A/cm^2$) are compared with that of single crystal TiO_2 rutile (in 1 N KOH at +0.00 V and $i_d = 0.0 \mu A/cm^2$). (The photospectra for the anodic films on titanium are multiplied ten times for visibility). It is apparent that the indirect bandgaps ($h\nu$ vs $\Phi^{1/2}$) shown in (b) that the anodic oxide on titanium is not rutile, but is proposed to be TiO_2 anatase.

is polarized at -0.60 V for one hour and then cycled between -1.1 and -0.3 V, photocurrent (1) (shown in Figure 10(b)) is obtained. If the iron is polarized at +0.00 V for one hour then cycled between -0.40 and +0.20 V, then photocurrent (2) is obtained. This suggests that there might be two distinct oxides on the surface of iron, which are stable over different potential regions. (These photocurrent curves are dependent on whether a fresh sur-

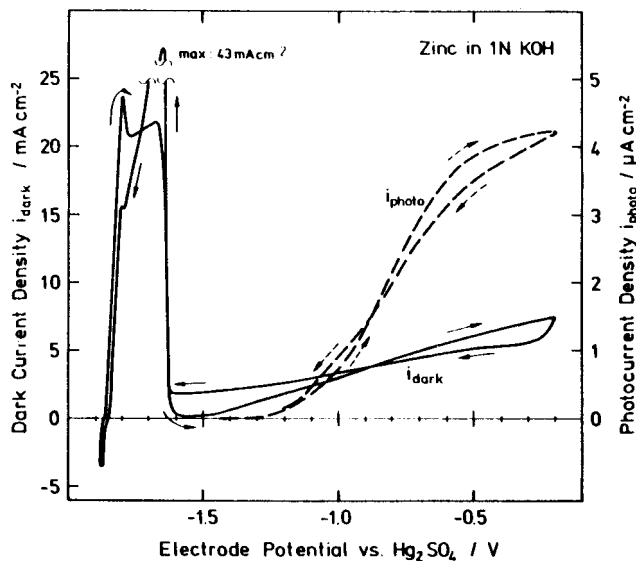


FIGURE 7. The cyclic voltammogram for zinc in 1 N KOH (10 mV/s, $\lambda = 350$ nm). The photocurrent onset occurs after the active region.

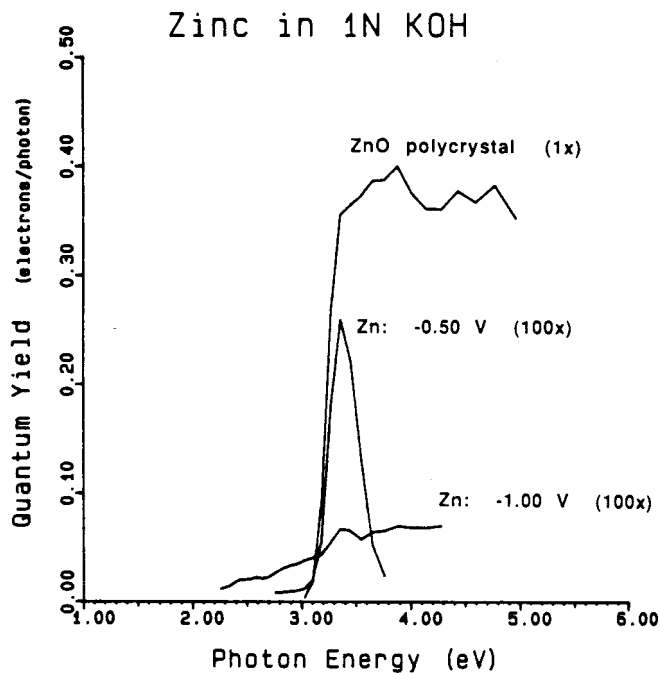


FIGURE 8. The photospectra for anodic oxide on zinc at -1.00 V (4 h and $i_d = 5.8 mA/cm^2$) and polycrystalline ZnO (2.5 h at -0.50 V and $i_d = 0.02 mA/cm^2$). It is seen that at higher voltages, the anodic oxide has the same E_g as polycrystalline ZnO.

face is polarized directly to -0.60 V or if it is cycled first before resting at the potential. When a fresh surface was polarized directly to -0.60 V, the photocurrent was too weak for a photospectra measurement.) The photospectra for these two oxides (after cycling) are shown in Figure 11. These two oxides in 1 N KOH, (1) and (2), might be $\delta-Fe(OH)_3$ and $\gamma-Fe_2O_3$, respectively. (Since there is no change in the dark current density, it is assumed that both oxides have the same valence state.) At low potentials, photocurrent (1) shows a "blue shift" in the indirect bandgap energy such that the E_g (indirect) gradually shifts from 2.5 to 2.3 eV as the voltage increases from -1.00 V to -0.60 V. The lower voltage film appears to have a larger E_g . This might result from a chang-

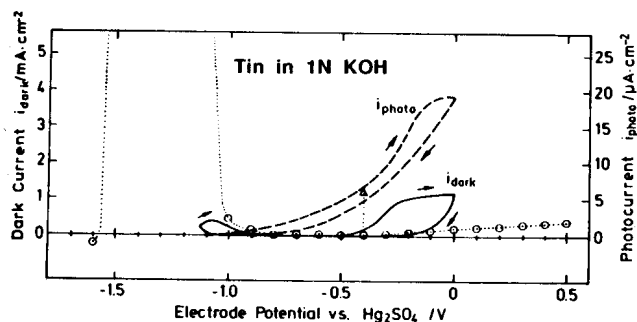
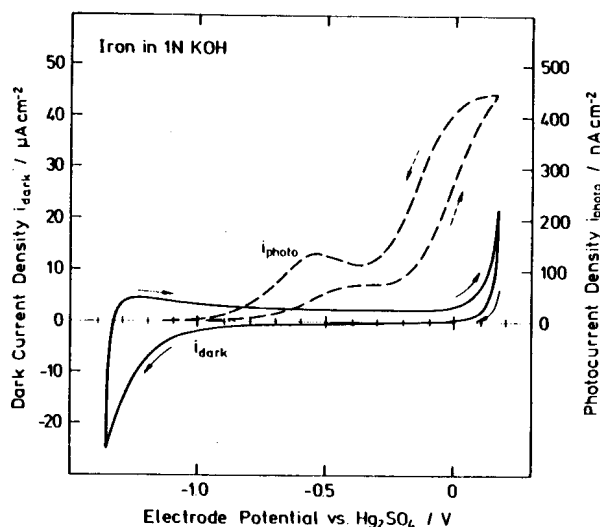
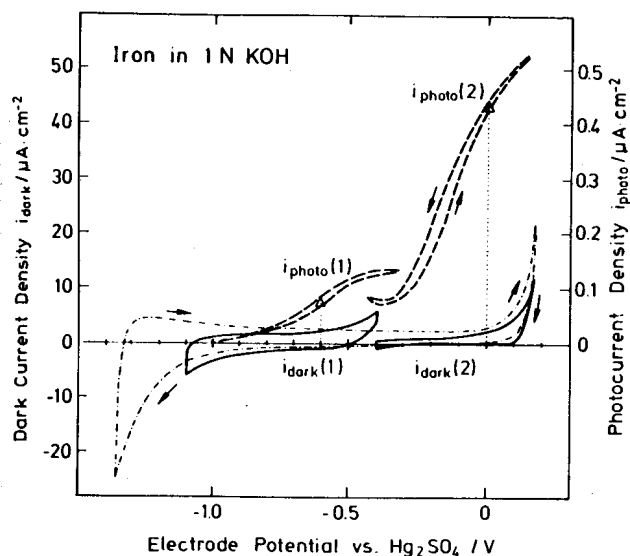


FIGURE 9. The cyclic voltammogram for tin in 1 N KOH under intense illumination (10 mV/s, $\lambda = 350$ nm, 2 mW/cm²). The dotted line is the potentiostatic polarization curve for tin in the dark. There is a large active dissolution region between -1.5 V and -1.0 V.



a



b

FIGURE 10. The cyclic voltammogram for iron in 1 N KOH (10 mV/s, $\lambda = 400$ nm). (a) There is a secondary maximum in the photocurrent near -0.5 V. By cycling within narrower regions, the photocurrent can be separated into two separate photocurrents (b), corresponding to two distinct oxides.

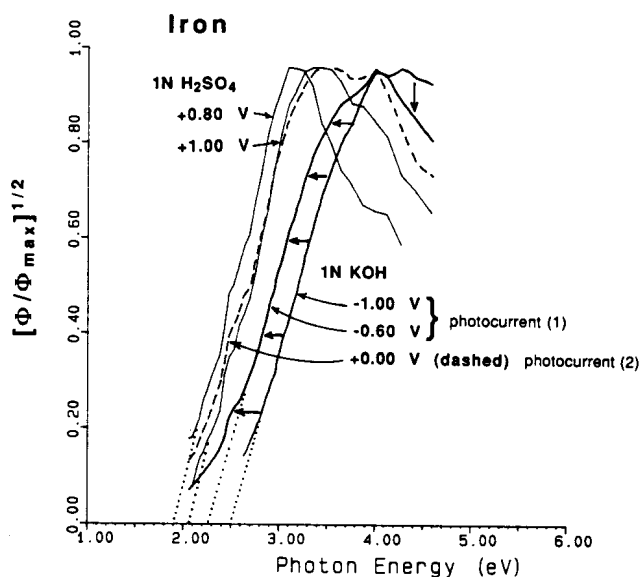


FIGURE 11. These photospectra ($h\nu$ vs $\Phi^{1/2}$) for iron are measured under focused light. In sulfuric acid there are two photospectra, one at $+0.80$ V (after 0.5 h, $i_d = 1$ mA/cm²) and the second at $+1.00$ V (after 2 h at $i_d = 4$ mA/cm²). In 1 N KOH there are also two spectras, photocurrent (1) at -0.60 V (after 1 h, $i_d < 0.05$ μ A/cm²) and photocurrent (2) at $+0.00$ V (after 1 h, $i_d = 1.5$ μ A/cm²). It can be seen that at higher potentials in 1 N sulfuric acid or in 1 N KOH, the same oxide exists on the surface of iron (probably γ -Fe₂O₃). At lower potentials, the oxides differ. In 1 N KOH, the photospectra shifts to lower energies as the voltage is increased from -1.00 V to -0.60 V.

ing composition of the thin film. These passive oxides have very low quantum yields, 0.1% or less.

The cyclic voltammogram for Fe in 1 N H₂SO₄ is shown in Figure 12. In sulfuric acid, iron exhibits a very large active region. The transition to passivity occurs near $+0.2$ V in the forward direction, and near -0.2 V in the reverse direction at a scan rate of 10 mV/s. The simultaneous photocurrent ($\lambda = 400$ nm) has a flat-band near 0.0 V. The dark passive current has a secondary peak near $+0.95$ V, which corresponds to a peak in the photocurrent as well. This probably signifies the formation of a new oxide with a different valence state. The photospectra for Fe in sulfuric acid are also shown in Figure 11. There are two separate spectra corresponding to the two different potentials, $+0.80$ V and $+1.00$ V. These might be Fe₃O₄ and γ -Fe₃O₄ respectively, in which the γ -Fe₃O₄ covers the Fe₃O₄, thus making the duplex oxide as proposed by Nagayama and Cohen.²⁴ Noteworthy, the photospectrum at $+1.00$ V in 1 N H₂SO₄ is practically identical to photocurrent (2) in 1 N KOH, confirming that at high potentials, the same oxide (probably γ -Fe₂O₃) exists on the surface of iron, whether at pH = 1 or pH = 14. (However, the lower potential oxide differs between the two solutions.) Much photoelectrochemical work has been done on the anodic film of passive iron. Stimming²⁵ has studied passive iron in acid, neutral, and base solutions and reported that the onset of photocurrent for the different solutions varies from photon energy 2.0 eV to 2.5 eV. Wilhelm and Hackerman²⁶ studied passive iron at pH = 8.4 and identified the flat-band potential (V_{fb}) and reported that the passive oxide was very similar to γ -Fe₂O₃. Azumi et al.²⁷ propose a band-structure for the passive film on iron in a neutral borate solution with a direct $E_g = 2.6$ eV and an indirect $E_g = 0.8$ eV.

Copper is not an active-passive metal. The cyclic voltammogram for copper in 1 N KOH is shown in Figure 13. The peak in the dark current at -0.6 V is not active dissolution but is a conversion peak of Cu⁺ to Cu²⁺.²⁸ This current maximum disappears in the potentiostatic measurement. The photocurrent ($\lambda = 400$ nm) in Figure 13(a) is negative and shows unusual but reproducible

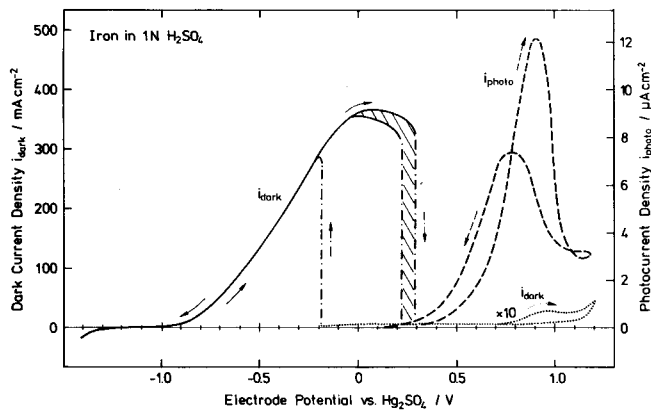


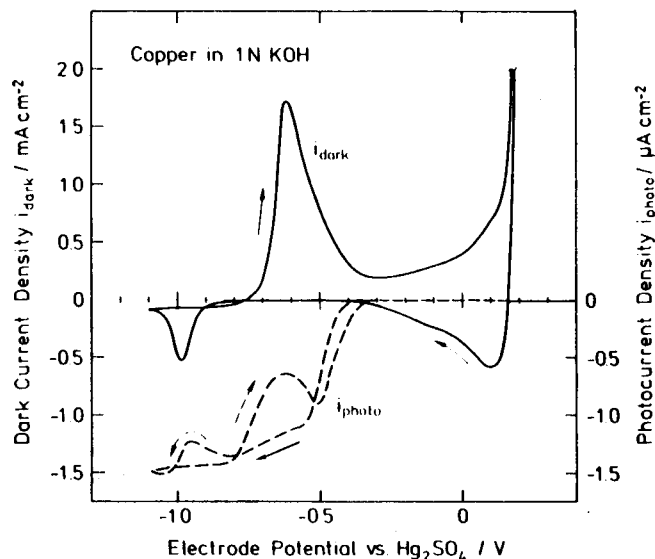
FIGURE 12. The cyclic voltammogram for iron in 1 N sulfuric acid (10 mV/s, $\lambda = 400$ nm) has both an active region and a passive region. The photocurrent onset occurs positive of the active region.

looping. The negative photocurrent is a result of the copper oxides, Cu_2O and CuO , being p-type, causing the energy bands at the surface to bend downward, thus reversing the electric field. Figure 13(b) shows that the photocurrent ($\lambda = 400$ nm) becomes much larger and almost reversible if it is cycled within a narrow region (note that the photocurrent scale is ten times larger). The larger photocurrent occurs because a single oxide is formed. Through experimentation, two regions are found where two distinct photocurrent curves become apparent, photocurrent (1) and photocurrent (2). The oxide for photocurrent (1) was reddish-brown and is interpreted as being Cu_2O . The oxide for photocurrent (2) was black and is interpreted as being CuO . Photospectra for these two oxides in oxygenated 1 N KOH are shown in Figure 14. The 1 N KOH was oxygenated by bubbling O_2 . When the solution was de-aerated, the photospectra were nonlinear and had poor reproducibility. In the oxygenated solution, the two oxides either became very stoichiometric, or else the electrons swept to the surface are consumed efficiently by the oxygen-reduction reaction. (Kruger and Calvert²⁹ previously reported that illumination causes dissolution of copper oxides in water. When they aerated the water, the effect of illumination was undetectable because of the higher dissolution rate.) In Table 1 are shown the apparent indirect bandgaps of the copper oxides. Cu_2O is 2.4 eV, which agrees with previous researchers (Stimming),³ but CuO is 1.1 to 1.7 eV, which does not agree. It should be noted that copper is nonpassive in 1 N KOH and the copper oxide continually thickens. Also noteworthy, although not shown here, is that in the regions where the surface oxide would be degenerate, the corrosion current becomes very noisy. Oxygen evolution begins on the degenerate CuO oxide (see Figure 13; the dark current increase occurs positive of where the photocurrent goes to zero). Much photoelectrochemical work has been done on copper: Bertocci³⁰ compared pure copper, Cu-Ni, and Cu-Al alloys in neutral solutions. Wilhelm et al.²⁸ reported on Cu_2O and CuO formed by anodic oxidation. DiQuarto et al.³¹ demonstrated the presence of n- Cu_2O in weakly acidic solutions. Pyun and Park³² demonstrated that hydroxides of Cu(I) and Cu(II) are initially formed, which then convert to copper oxides upon aging.

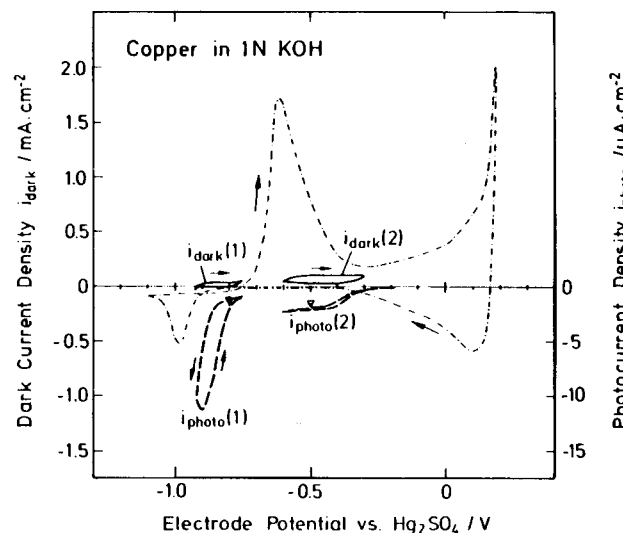
Similar photo-experiments were attempted with nickel, chromium, manganese and cobalt, but with unsatisfactory results. Either this experimental technique is invalid for these anodic oxides, or else the photocurrent mechanism (shown in Figure 1) is invalid. However, this method and mechanism are valid for Pb and Cd (see also Peter)⁴ although the results are not shown here.

DISCUSSION

Photoelectrochemistry can be used to identify the anodic ox-



a



b

FIGURE 13. The cyclic voltammogram for copper in 1 N KOH (20 mV/s, $\lambda = 400$ nm) has a negative and looping photocurrent in (a). In (b), by cycling within narrow regions, two distinct photocurrents, (1) and (2), are resolved. These correspond to Cu_2O and CuO respectively.

ides that form on metals. The anodic oxides can be characterized by their bandgap energy (E_g) and flat-band potential (V_{fb}). It is assumed that a given oxide (or hydroxide) with a given structure will have a unique bandgap. The flat-band potential might vary since it can change with the doping level of the oxide. Table 1 lists E_g and V_{fb} for most of the oxides studied in this paper. Additionally, this work has shown that if the photocurrent voltammogram is irreversible or has a maximum, it can indicate the formation of a new oxide (see Cu, Fe or Sn).⁸

After comparing the photocurrents and the corrosion currents of passive and active-passive metals, a possible relationship is observed: The anodic oxides appear to be nonprotective when they are degenerate. (Degeneracy is defined as the condition when the conduction [or valence] bands of a semiconductor bend across its Fermi level. In the degenerate state the oxide [semiconductor] becomes an electronic conductor.)³³ The metals (Fe, Zn, Sn) that exhibit active dissolution are postulated to have degenerate oxides in their active regions. This can be seen for zinc in Fig-

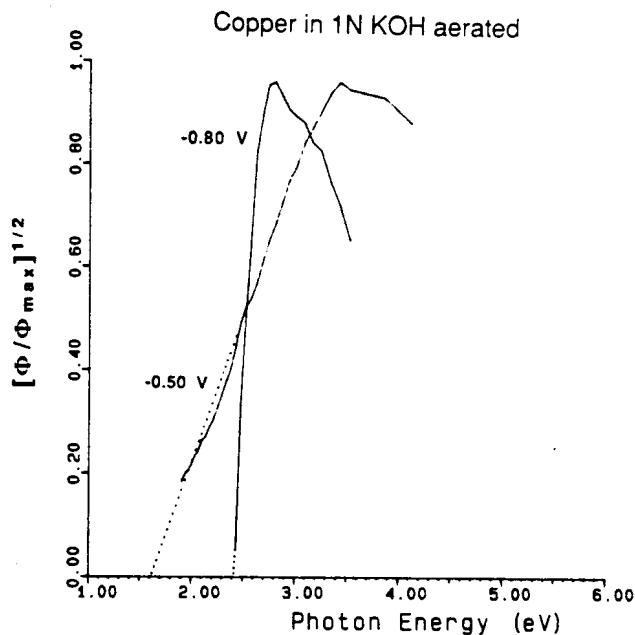


FIGURE 14. The photospectra for copper in 1 N KOH varies if the solution is aerated or deaerated. The aerated solutions produce very linear curves for the indirect E_g ($h\nu$ vs $\Phi^{1/2}$) both at -0.80 V ($i_d = -266 \mu\text{A}/\text{cm}^2$), and at -0.50 V ($i_d = +8.3 \mu\text{A}/\text{cm}^2$). The deaerated solution (not shown) exhibited poor reproducibility and nonlinearity.

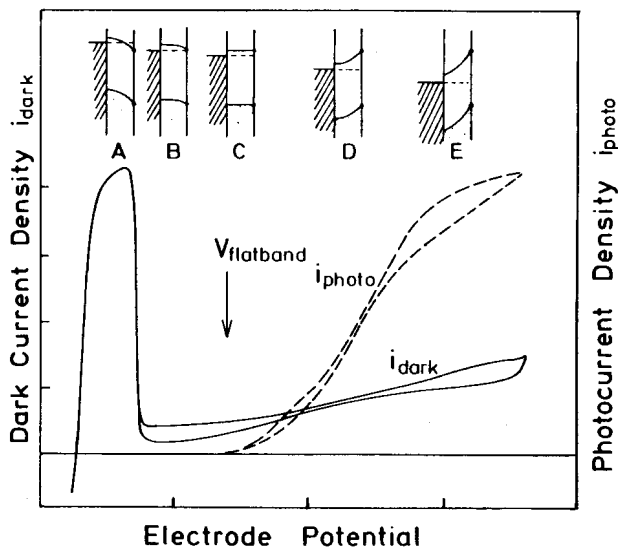


FIGURE 15. A postulated model of the band-bending in the oxide film is shown above the photocurrent and corrosion current voltammograms. The passive region corresponds to band-bending upward (depletion zone). In the active region, the bands bend downward and intersect the Fermi level (degeneracy). This degenerate state is postulated to assist active dissolution.

ure 7, for tin in Figure 9, and for iron in sulfuric acid in Figure 12. In these figures, the photocurrent does not begin until potentials more noble than the active-passive transition. Figure 15 illustrates this concept. In the active region A, the energy bands are bent downward so that the Fermi level cuts through the conduction band. This is a degenerate oxide (in accumulation) and apparently is nonprotective, allowing the dissolution of the underlying metal. In region B, the energy bands are still bent downward, but not below the Fermi level. Passivity begins at this point. The accumulation in region B does not usually cause a significant negative pho-

tocurrent because the charged region is usually too narrow. In region C, the energy bands are flat, thus the so-named "flat-band potential" (V_{fb}) where the photocurrent onset occurs. In regions D and E, the energy bands bend upward, causing the electric field and the positive photocurrent. The larger electric field (and depletion region) in region E causes the correspondingly larger photocurrent. It is postulated that zirconium (Figure 3), titanium (Figure 5), and iron in 1 N KOH (Figure 10) do not have active regions because their respective oxides are never degenerate during anodic potentials. (Figure 15 could probably be extended for some passive films into the transpassive region in which severe band-bending would cause degeneracy (in inversion) by the valence bands crossing the Fermi level. The degenerate transpassive oxide would be a electric conductor that would aid oxygen evolution and breakdown.)

Verification of Figure 15 can be found in the work of Pinkowski who modeled the passive oxide of iron as a graded PIN junction.³⁴ Pinkowski demonstrated that the experimental capacitance/potential curves (at pH = 8.4) could be theoretically explained by band-bending causing degeneracy of the PIN junction. Comparing Pinkowski's data³⁴ with Sato's corrosion data³⁵ (at pH = 8.4) shows that the active region corresponds to the oxide degenerate in accumulation, while the transpassive region corresponds to the oxide degenerate in inversion. Pinkowski,³⁴ however, did not draw any connection between the corrosion currents and the degeneracy.

CONCLUSION

► Photocurrents generated from anodic oxides on metals carry with them valuable information about the anodic oxide. Analysis can give the flat-band potential (V_{fb}) and the bandgap energy (E_g), which can be used to identify the oxide. Irreversible photocurrent voltammograms appear to indicate the formation of secondary oxides. Experimentally it is observed that the region of active dissolution lies negative of the region of zero photocurrent. In the active region, the anodic oxide on the metal would be degenerate (the oxide's energy bands would bend so that the Fermi level would be within the conduction band). It is postulated that the degenerate anodic oxide corresponds to the nonprotective oxide that allows active dissolution of the base metal.

ACKNOWLEDGMENTS

I thank the Alexander-von-Humboldt Foundation of West Germany for my research fellowship, Professor Heinz Gerischer for discussions, Michael Butler for information on anatase, Norbert Sorg for the polycrystalline ZnO, and Sabine Wasle and Margot Lübke for many of the drawings.

REFERENCES

1. E.K. Oshe and I.L. Rosenfel'd, Doklady Phys. Chem., 194(1969): pp. 71-74.
2. F.M. Delnick and N. Hackerman, Passivity of Metals, eds. R.P. Frankenthal and J. Kruger, (Pennington, NJ: Electrochem. Soc., 1976), pp. 116-123.
3. U. Stimming, Electrochimica Acta 31,4(1986): pp. 415-429.
4. L.M. Peter, Ber. Bunsenges. Phys. Chem. 91(1987): pp. 419-426.
5. A.K. Vijk, Corro. Sci. 12(1972): pp. 105-111.
6. N. Sato, J. Electrochem. Soc., 128,2(1982): pp. 255-280.
7. T.D. Burleigh and R.M. Latanision, Corrosion 43,8(1987): pp. 471-475.
8. T.D. Burleigh and H. Gerischer, J. Electrochem. Soc. 135,12(1988): pp. 2938-2942.
9. H. Gerischer, J. Electrochem. Soc. 134,11(1966): 1174-1181.
10. H. Gerischer, Corro. Sci. 29,2/3(1989): pp. 257-266.
11. W.H. Strehlow and E.L. Cook, J. Phys. Chem. Ref. Data. 2,1(1973): pp. 163-199.
12. T.D. Burleigh and R.M. Latanision, J. Electrochem. Soc. 134,1(1987): pp. 136-138.
13. J.W. Schultze, U. Stimming, and J. Weise, Ber. Bunsenges. Phys. Chem. 86(1982): pp. 276-282.
14. K. Leitner, J.W. Schultze, and U. Stimming, J. Electrochem. Soc., 133,8(1986): pp. 1561-1568.

15. D.C. Cronemeyer, *Phys. Rev.* 87,5(1952): pp. 876-886.
16. V.B. Gusev, L.M. Lenev, and I.I. Kalinichenko, *Zh. Prikl. Spektrosk.* 34,5(1981): pp. 939-941.
17. R.J.H. Clark, in *Comprehensive Inorganic Chemistry*, ed. A.F. Trotman-Dickenson (Oxford, England: Pergamon Press Ltd., 1973), pp. 375-377.
18. G. Blondeau, M. Froehlicher, M. Froment et al., *J. Microsc. Spectro. Elect.* 2,1(1977): pp. 27-38.
19. J. Yahalom and J. Zahavi, *Electrochimica Acta* 15(1970): pp. 1429-1435.
20. M. R. Kozlowski, P.S. Tyler, W.H. Smyrl, and R.T. Atanasoski, *Surf. Sci.* 194(1988): pp. 505-530.
21. S.-E. Lindquist, A. Lingren, and Zhu Yan-Ning, *J. Electrochem. Soc.* 132,3(1985): pp. 623-631.
22. O. Fruhwirth, G.W. Herzog, and J. Poulkous, *Surf. Tech.* 11(1980): pp. 259-267.
23. S. Kapusta and N. Hackerman, *Electrochim. Acta* 25(1980): pp. 1001-1006.
24. M. Nagayama and M. Cohen, *J. Electrochem. Soc.* 109,9(1962): pp. 781-790.
25. U. Stimming, in *Passivity of Metals and Semiconductors*, ed. M. Froment, (Amsterdam, the Netherlands: Elsevier Sci. Publ., 1983), pp. 477-482.
26. S.M. Wilhelm and N. Hackerman, *J. Electrochem. Soc.* 128,8(1981): pp. 1668-1674.
27. K.Azumi, T. Ohtsuka, and N. Sato, *J. Electrochem. Soc.* 133,7(1986): pp. 1326-1328.
28. S.M. Wilhelm, Y. Tanizawa, Chang-Yi Liu, and N. Hackerman, *Corro. Sci.* 22,8(1982): pp. 791-805.
29. J. Kruger and J.P. Calvert, *J. Electrochem. Soc.* 111,9(1964): pp. 1038-1041.
30. U. Bertocci, *J. Electrochem. Soc.* 125,10(1978): pp. 1598-1602.
31. F. DiQuarto, S. Piazza, and C. Sunseri, *Electrochim. Acta*, 30,3(1985): pp. 315-324.
32. C.-H. Pyun and S.-M. Park, *J. Electrochem. Soc.* 133,10(1986): pp. 2024-2030.
33. S.R. Morrison, *Electrochemistry at Semiconductor and Oxidized Metal Electrodes* (New York, NY: Plenum Press, 1980), pp. 49-78.
34. A. Pinkowski, *Z. Phys. Chemie, Leipzig* 267(1986): pp. 718-722.
35. N. Sato, in *Passivity of Metals*, ed. R.P. Frankenthal and J. Kruger, (Pennington, NJ: Electrochem. Soc. Inc., 1978), p. 31.

Electrochemical Behavior of Copper in 0.5 M H₂SO₄ Solutions in the Absence and Presence of Fe(III) and Benzotriazole [☆]

S.L.F.A. da Costa and S.M.L. Agostinho*

ABSTRACT

The electrochemical behavior of copper in 0.5 M deaerated sulfuric acid in the absence and presence of benzotriazole (BTAH) and ferric ions has been investigated with rotating disk electrodes.

The BTAH inhibitive effect initiates at concentrations as low as 10⁻⁷ M.

The mechanism of Cu/Cu(II) reaction is the same in the absence and presence of low BTAH concentrations (<10⁻⁵ M). For higher inhibitor concentrations, different processes must be considered to understand the interface metal-solution behavior: the formation of a Cu(I)BTA film, the presence of disproportionation reaction Cu + Cu(II) → 2Cu(I) and the complexation of Cu(II) ions by BTAH.

The presence of Fe(III) ions in 0.5 M H₂SO₄ does not affect the anodic dissolution of copper. However, in the presence of BTAH, the addition of Fe(III) makes the inhibitor less effective.

From anodic polarization measurements at constant potential the film adsorption has been evaluated by using the Langmuir adsorption isotherm.

INTRODUCTION

In a previous work¹ BTAH has been reported to inhibit effectively the corrosion of copper by ferric ions in 0.5 M H₂SO₄ solutions. The corrosion process is diffusion controlled by Fe(III) ions to the electrode surface in the absence and presence of BTAH. The in-

hibitor adsorption follows Langmuir behavior with an adsorption equilibrium constant of 8.8 × 10³ M⁻¹. The corrosion ceases completely at BTAH concentration of 5 mM and the protective layer is composed of [Cu(I)BTA] complex.

Power et al.² taking into account the relationships between the corrosion potential and ferric ion concentration and angular velocity of copper disks immersed in 0.1 M H₂SO₄ solutions containing Fe(III) elucidated the mechanism of the corrosion process. An anodic Tafel slope of around 39 mV/decade was found which is consistent with a two steps of one-electron mechanism.^{3,4,5} This mechanism was well defined for copper dissolution in noncomplexing media through polarization data by Mattson and Bockris⁶ and Losev et al.⁷ Wu and Nobe⁸ studied the effect of substituted benzotriazoles (0.2 mM) on the anodic dissolution of copper in 0.5 M H₂SO₄ solutions at very low polarizations. BTAH has been reported to inhibit the copper dissolution reaction. The Tafel slope for the uninhibited copper was 35 mV/decade and for the inhibited one it was 60 mV/decade.

The objectives of the present work are: (1) to investigate the effect of BTAH on the open-circuit characteristics of rotating copper disks in 0.5 M H₂SO₄ solutions containing Fe(III) ions at various rotation frequencies, (2) to examine the effect of low BTAH concentrations (10⁻⁷ to 10⁻⁵ M) on the anodic behavior of copper in 0.5 M H₂SO₄ solutions, (3) to verify the effect of Fe(III) ions on the anodic polarization behavior of copper in 0.5 M H₂SO₄ solutions, (4) to investigate the inhibiting action of BTAH on the anodic behavior of copper in the presence of Fe(III) ions, and (5) to obtain the Langmuir isotherm of the protective film from anodic polarization of copper in the presence of BTAH without Fe(III) ions and to compare these results with the previous one obtained by weight loss experiments.¹

* Submitted for publication September 1987; revised September 1988.

* Instituto de Quimica da Universidade de Sao Paulo, C.P. 20780, 01498-Sao Paulo, Brazil.